1

General Impact of Translational Symmetry in Crystals on Solid State Physics

Atomic order in crystals.
Local and translational symmetries.
Symmetry impact on physical properties in crystals.
Wave propagation in periodic media.
Quasi-momentum conservation law.
Reciprocal space.
Wave diffraction conditions.
Degeneracy of electron energy states at the Brillouin zone boundary.
Diffraction of valence electrons and bandgap formation.

In contrast to liquids or gases, atoms in a solid state, in average (over time), are located at fixed atomic positions. The thermally assisted movements around them or between them are strongly limited in space (as for thermal vibrations in potential wells) or have rather low probabilities (as for long-range atomic diffusion). According to the types of the averaged long-range atomic arrangements, all solid materials can be sub-divided into the three following classes, i.e. regular crystals, amorphous materials, and quasicrystals.

Most solid materials are regular (conventional) crystals with fully ordered and periodic atomic arrangements, which can be described by the set of translated elementary blocks (unit cells) densely covering the space with no voids. Nowadays, using the advanced characterization methods, such as high-resolution electron microscopy or scanning tunneling microscopy, it is possible to directly visualize this atomic periodicity (Figure 1.1). Due to the translational symmetry, the key phenomenon – namely, diffraction of short-wavelength quantum beams (electrons, X-rays, neutrons) – takes place. As we show in the following text, sharp diffraction peaks (or spots), which are the "visiting card" of crystalline state, are originated from the quasi-momentum (quasi-wavevector) conservation law in 3D.

In contrary, amorphous materials, being characterized by some kind of short-range ordering, do not reveal atomic order on a long range (Figure 1.2). In other words, certain correlations between atomic positions exist within a few first coordination spheres only and rapidly attenuate and disappear at longer distances.

Introduction to Solid State Physics for Materials Engineers, First Edition. Emil Zolotoyabko.

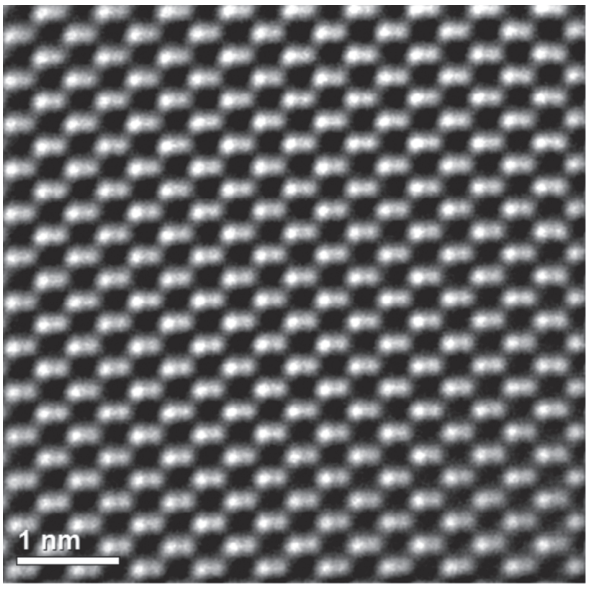

Figure 1.1 High-resolution scanning transmission electron microscopy image of atomic columns in crystalline GaSb. Cations and anions within dumbbells are separated by 0.15 nm.

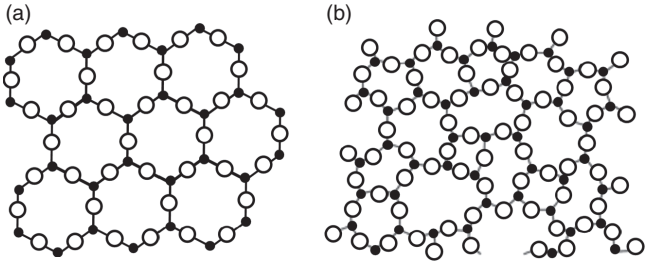

Figure 1.2 Structural motifs in silicon dioxide (SiO_2): (a) – ordered atomic arrangement in crystalline quartz; (b) – disordered arrangement in amorphous silica. Large open circles and black filled circles indicate oxygen and silicon atoms, respectively.

Correspondingly, diffraction patterns taken from amorphs show diffuse features only (called amorphous halo), rather than sharp diffraction peaks.

Quasicrystals in some sense occupy a niche between crystals and amorphs. They have been discovered in the beginning of 1980s by **Dan Shechtman** during his studies (by electron diffraction) of the structure of rapidly solidified Al–Mn alloys. Quasicrystals can be described as fully ordered, *but non-periodic arrangements* of elementary blocks densely covering the space with no voids. An example of filling the 2D space in this fashion, by the so-called **Penrose** tiles (rhombs having smaller angles equal 18° and 72°), is shown in Figure 1.3. Amazingly that despite the lack of the long-range translational symmetry, quasicrystals, like regular crystals, also produce sharp diffraction peaks (or spots), their positions being defined by the quasi-momentum conservation law in high-dimensional space (higher than 3D, see Section 1.1). In this high-dimensional space (hyperspace), quasicrystals are periodic entities, their periodicity being lost when projecting them onto real 3D space.

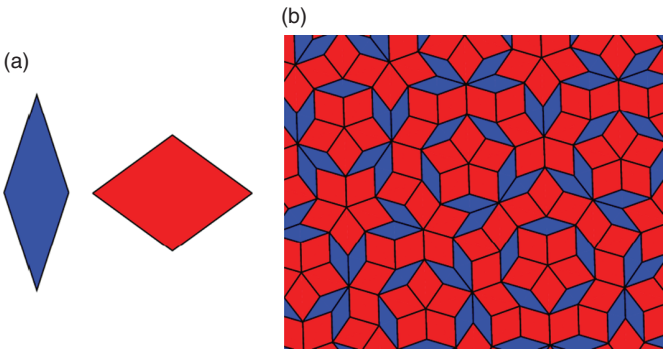

Figure 1.3 Dense filling of 2D space by spatially ordered, though non-periodic **Penrose** tiles (b). Fivefold symmetry regions (regular pentagons) are clearly seen across the pattern. Elemental shapes composing this tiling, i.e. two rhombs with smaller angles equal 18° (blue) and 72° (red), are shown in the (a).

In 1992, based on these findings, the International Union of Crystallography changed the definition of a crystal toward uniting the regular crystals and quasicrystals under single title with an emphasis on the similarity of diffraction phenomena: "A material is a crystal if it has *essentially* a sharp diffraction pattern. The word *essentially* means that most of the intensity of the diffraction is concentrated in relatively sharp **Bragg** peaks, besides the always present diffuse scattering." In 2011, **Dan Shechtman** was awarded Nobel Prize in Chemistry "for the discovery of quasicrystals."

1.1 Crystal Symmetry in Real Space

Across this book, we will focus on physical properties of regular crystals, amorphs and quasicrystals being out of our scope here. Thinking on conventional crystals, we first keep in mind their translational symmetry. As we already mentioned, the long-range periodic order in crystals leads to translational symmetry, which is commonly described in terms of **Bravais** lattices (named after French crystallographer **Auguste Bravais**):

$$\boldsymbol{r_s} = n_1\boldsymbol{a_1} + n_2\boldsymbol{a_2} + n_3\boldsymbol{a_3} \tag{1.1}$$

The nodes, $\boldsymbol{r_s}$, of **Bravais** lattice are produced by linear combinations of three non-coplanar vectors, $\boldsymbol{a_1}$, $\boldsymbol{a_2}$, $\boldsymbol{a_3}$, called translation vectors. The integer numbers in Eq. (1.1) can be positive, negative, or zero. Atomic arrangements within every crystal can be described by the set of analogous **Bravais** lattices.

Classification of **Bravais** lattices is based on the relationships between the lengths of translation vectors, $|\boldsymbol{a_1}| = a$, $|\boldsymbol{a_2}| = b$, $|\boldsymbol{a_3}| = c$ and the angles, α, β, γ, between them. In fact, all possible types of **Bravais** lattices can be attributed to seven symmetry systems:

Triclinic: $a \neq b \neq c$ and $\alpha \neq \beta \neq \gamma$;

Monoclinic: $a \neq b \neq c$ and $\alpha = \beta = 90°$, $\gamma \neq 90°$; in this setting, angle γ is between translation vectors $\boldsymbol{a}_1$ ($|\boldsymbol{a}_1| = a$) and $\boldsymbol{a}_2$ ($|\boldsymbol{a}_2| = b$); whereas the angles α and β are, respectively, between translation vectors $\boldsymbol{a}_2 \wedge \boldsymbol{a}_3$ and $\boldsymbol{a}_1 \wedge \boldsymbol{a}_3$;

Orthorhombic : $a \neq b \neq c$ and $\alpha = \beta = \gamma = 90°$;

Tetragonal: $a = b \neq c$ and $\alpha = \beta = \gamma = 90°$;

Cubic: $a = b = c$ and $\alpha = \beta = \gamma = 90°$;

Rhombohedral: $a = b = c$ and $\alpha = \beta = \gamma \neq 90°$;

Hexagonal: $a = b \neq c$ and $\alpha = \beta = 90°$, $\gamma = 120°$.

A parallelepiped built by the aid of vectors $\boldsymbol{a}_1$, $\boldsymbol{a}_2$, $\boldsymbol{a}_3$ is called a unit cell and is the smallest block, which being duplicated by the translation vectors allows us to densely fill the 3D space without voids.

Translational symmetry, however, is only a part of the whole symmetry in crystals. Atomic networks, described by **Bravais** lattices, also possess the so-called local (point) symmetry, which includes lattice inversion with respect to certain lattice points, mirror reflections in some lattice planes, and lattice rotations about certain rotation axes (certain crystallographic directions). After application of all these symmetry elements, the lattice remains invariant. Furthermore, rotation axes are defined by their order, n. The latter, in turn, determines the minimum angle, $\varphi = \frac{360°}{n}$, after rotation by which the lattice remains indistinguishable with respect to its initial setting (lattice invariance). In regular crystals, the permitted rotation axes, i.e. those matching translational symmetry (see Appendix 1.A), are twofold (180°-rotation, $n = 2$), threefold (120°-rotation, $n = 3$), fourfold (90°-rotation, $n = 4$), and sixfold (60°-rotation, $n = 6$). Of course, onefold, i.e. 360°-rotation ($n = 1$), is a trivial symmetry element existing in every **Bravais** lattice. The international notations for these symmetry elements are: $\bar{1}$– for inversion center, m – for mirror plane, and *1*, *2*, *3*, *4*, *6* – for respective rotation axes. We see that fivefold rotation axis and axes of the order, higher than $n = 6$, are incompatible with translational symmetry (see Appendix 1.A).

To deeper understand why some rotation axes are permitted, while others not, let us consider the covering of the 2D space by regular geometrical figures, having n equal edges and central angle, $\varphi = \frac{360°}{n}$ (Figure 1.4). Correspondingly, the angle, δ, between adjacent edges is:

$$\delta = 180° - \varphi = 180° - \frac{360°}{n} \tag{1.2}$$

To produce a pattern without voids by using these figures, we require that the full angle around each meeting point, M, defined by p adjacent figures, should be 360°, i.e. $p \cdot \delta = 360°$. Therefore, using Eq. (1.2) yields:

$$p\delta = p\left[180° - \frac{360°}{n}\right] = 360° \tag{1.3}$$

or

$$\frac{1}{2} - \frac{1}{n} = \frac{1}{p} \tag{1.4}$$

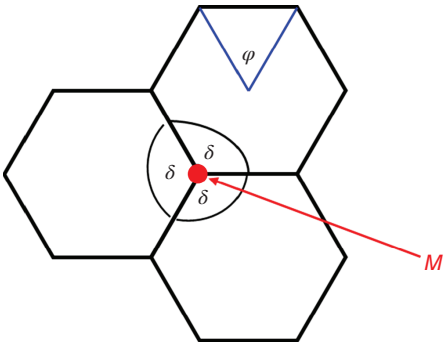

Figure 1.4 Dense filling of 2D space by regular geometrical figures.

Finally, we obtain:

$$p = \frac{2n}{n-2} = 2 + \frac{4}{n-2} \tag{1.5}$$

It follows from Eq. (1.5) that there is a very limited set of regular figures (with $2 < n \leq 6$) useful for producing periodic patterns, which fill the 2D space with no voids (i.e. providing integer numbers, p). These are hexagons ($n = 6$, $p = 3$, $\varphi = 60°$), squares ($n = 4$, $p = 4$, $\varphi = 90°$), and triangles ($n = 3$, $m = 6$, $\varphi = 120°$). Based on the value of central angle, φ, these regular figures possess the sixfold, fourfold, and threefold rotation axes, respectively. Since they are related to regular geometrical figures, these rotation axes are called high-symmetry elements. Regarding the twofold axis, it fits the symmetry of the parallelogram, which also can be used for filling the 2D space without voids but does not represent a regular geometrical figure. For this reason, the twofold rotation axis is classified as a low symmetry element (together with inversion center, $\bar{1}$, and mirror plane, m). It also comes out from Eq. (1.5), that regular figures with fivefold rotation axis ($n = 5$), as well as with rotation axes higher than $n > 6$, are incompatible with translational symmetry, i.e. cannot be used for producing periodic patterns without voids since parameter, p, is not an integer number.

In the absence of the long-range translational symmetry, however, as in quasicrystals, one can find additional rotation axes, e.g. fivefold ($\varphi = \frac{360°}{5} = 72°$), as for 2D construction shown in Figure 1.3 or for icosahedral symmetry in 3D. The latter can be found in two **Platonic** bodies: regular icosahedrons and dodecahedrons. Regular dodecahedron has 12 pentagonal faces and 20 vertices, in each of them three faces meet (Figure 1.5). Therefore, the fivefold axes are normal to the pentagonal faces. In contrast, regular icosahedron has 20 triangular faces and 12 vertices, in each of them five faces meet (Figure 1.6). Therefore, the fivefold axes connect the body center and each vertex. Note that regular pentagon (plane figure) has central angle 72° and is characterized by the so-called golden ratio τ (the ratio between the pentagon diagonal, d_p, and pentagon edge, a_p, see Figure 1.7):

$$\tau = \frac{d_p}{a_p} = 2\cos 36° = \frac{1+\sqrt{5}}{2} = 1.681 \tag{1.6}$$

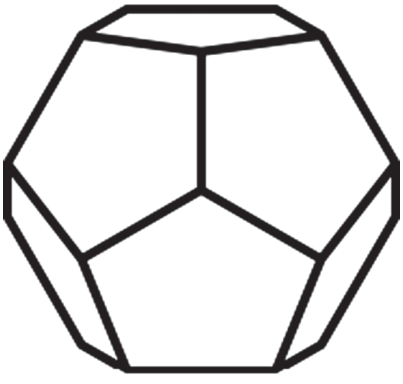

Figure 1.5 Dodecahedron sculpted by 12 pentagonal faces.

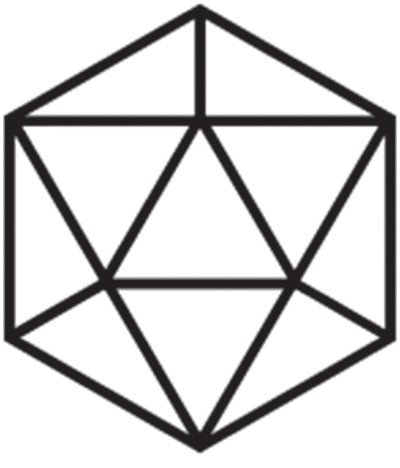

Figure 1.6 Icosahedron sculpted by 20 triangular faces.

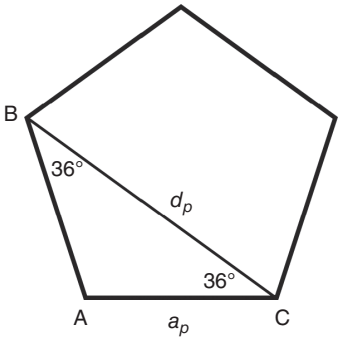

Figure 1.7 Regular pentagon with edges equal a_p and diagonals equal d_p. The ratio, $\frac{\mathrm{BC}}{\mathrm{AC}} = \frac{d_p}{a_p} = 2\cos 36° = \frac{1+\sqrt{5}}{2}$, is called the golden ratio (Eq. (1.6)).

which is of great importance to the quasicrystal diffraction conditions (described later in this chapter).

Permitted combinations of local symmetry elements (totally 32 in regular crystals) are called point groups. A set of different crystals, possessing the same point group symmetry, form certain crystal class. Point group symmetry is responsible for

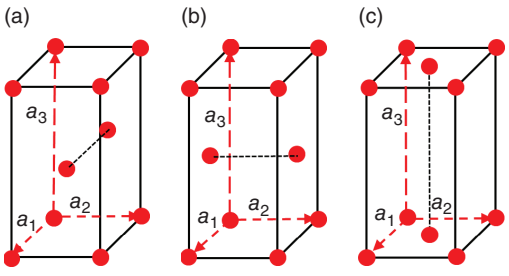

Figure 1.8 Unit cells of the following side-centered **Bravais** lattices: A-type (a), B-type (b), C-type (c). Translation vectors, $\boldsymbol{a_1}$, $\boldsymbol{a_2}$, $\boldsymbol{a_3}$, are indicated by dashed arrows.

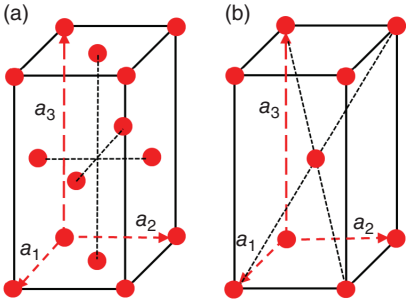

Figure 1.9 Unit cells of the following centered **Bravais** lattices: (a) face-centered (F-type) and (b) body-centered (I-type). Translation vectors, $\boldsymbol{a_1}$, $\boldsymbol{a_2}$, $\boldsymbol{a_3}$, are indicated by dashed arrows.

anisotropy of physical properties in crystals, as explained in more detail further in this chapter.

Bravais lattices defined by Eq. (1.1) are primitive (P) since they effectively contain only one atom per unit cell. However, in some symmetry systems, the same local symmetry will be held for centered **Bravais** lattices, in which the symmetry-related equivalent points are not only the corners (vertices) of the unit cell (as for primitive lattice), but also the centers of the unit cell faces or the geometrical center of the unit cell itself (Figures 1.8 and 1.9). Such lattices are conventionally called *side-centered* (A, B, or C), *face-centered* (F), and *body-centered* (I). In side-centered modifications of the type A, B, or C, additional equivalent points are in the centers of two opposite faces, being perpendicular, respectively, to the $\boldsymbol{a_1}$-, $\boldsymbol{a_2}$-, or $\boldsymbol{a_3}$- translation vectors (Figure 1.8). In the face-centered modification, F, all faces of the **Bravais** parallelepiped (unit cell) are centered (Figure 1.9). For the cubic symmetry system, the F-centered **Bravais** lattice is called face-centered cubic (fcc). In the body-centered modification, I, the center of the unit cell is symmetry-equivalent to the unit cell vertices (Figure 1.9). For the cubic symmetry system, the I-modification of the **Bravais** lattice is called body-centered cubic (bcc). Accounting of centered **Bravais** lattices increases their total amount up to 14.

In some cases, the choice of **Bravais** lattice is not unique. For example, fcc lattice can be represented as rhombohedral one with $a_R = a/\sqrt{2}$ and $\alpha = 60°$ (Figure 1.10a). Rhombohedral lattice is a primitive one and comprises one atom per unit cell instead four atoms in the fcc unit cell. Similarly, bcc lattice can be represented in the rhombohedral setting with $a_R = a\sqrt{3}/2$ and $\alpha = 109.47°$ (Figure 1.10b). In this case, the rhombohedral lattice comprises one atom per unit cell instead two atoms in the bcc

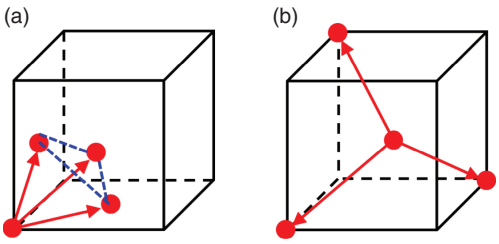

Figure 1.10 Lattice translations (red arrows) in the rhombohedral setting of the fcc (a) and bcc (b) lattices.

Table 1.1 Summary of possible symmetries in regular crystals.

Crystal symmetry	Bravais lattice type	Crystal classes (point groups)
Triclinic	P	1, $\bar{1}$
Monoclinic	P; B, or C	m, 2, 2/m
Orthorhombic	P; A, B, or C; I; F	$mm2$, 222, mmm
Tetragonal	P; I	4, 422, $\bar{4}$, $\bar{4}2m$, 4/m, 4mm, 4/mmm
Cubic	P; I (bcc); F (fcc)	23, $m\bar{3}$, 432, $\bar{4}3m$, $m\bar{3}m$
Rhombohedral (trigonal)	P (R)	3, 32, 3m, $\bar{3}$, $\bar{3}m$
Hexagonal	P	6, 622, $\bar{6}$, $\bar{6}2m$, 6/m, 6mm, 6/mmm

unit cell. We will widely use these settings in Chapter 2 considering the shapes of **Brillouin** zones. Minimizing number of atoms in the unit cell substantially reduces the calculation complexity of different physical properties in crystals.

Symmetry systems, types of **Bravais** lattices, and distribution of crystal classes (point groups) among them are summarized in Table 1.1.

The number of high-order symmetry elements, i.e. the threefold, fourfold, and sixfold rotation axes, which can simultaneously appear in a crystal, is also symmetry limited. For threefold rotation axis, this number may be one, in trigonal classes, or four, in cubic classes; for fourfold rotation axes – one in tetragonal classes or three in some cubic classes, while for sixfold rotation axis – only one in all hexagonal classes (see Appendix 1.A).

The presence or absence of an inversion center in a crystal is of upmost importance to many physical properties. For example, ferroelectricity and piezoelectricity (see Chapter 12) do not exist in centro-symmetric crystals, i.e. in those having inversion center. In this context, it is worth to note that any **Bravais** lattice is centro-symmetric. For primitive lattices, this conclusion follows straightforwardly from Eq. (1.1). Centered (non-primitive) **Bravais** lattices certainly do not refute this statement (Figures 1.8 and 1.9). However, only 11 crystal classes of total 32, in fact, are centro-symmetric. Even for high cubic symmetry, only two classes are centro-symmetric, i.e. $m\bar{3}$ and $m\bar{3}m$ (Table 1.1). Evidently, the loss of an inversion center can happen in crystals, which are built of several **Bravais** lattices, their origins being shifted relative to each other. We stress that it is necessary, but not

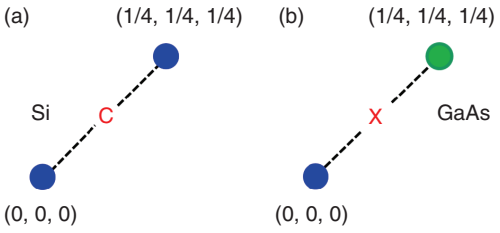

Figure 1.11 The presence of inversion center (**C**) in diamond structure (a) and its loss (**X**) in zinc-blende structure (b). Dissimilar atoms are indicated by different colors.

sufficient condition for the loss of inversion center. For illustration, let us consider Si (diamond structure) and GaAs (zinc blende or sphalerite structure) crystals. Both comprise two fcc lattices shifted relative to each other by one quarter of a space cube diagonal. The difference is that in silicon these sub-lattices are occupied by identical atoms (Si), whereas in GaAs – separately by Ga and As. In a result, Si is centro-symmetric (class $m\bar{3}m$) that can be easily proved by setting inversion center at point $(1/8, 1/8, 1/8)$, i.e. in the middle between the origins of two centro-symmetric fcc Si sub-lattices (Figure 1.11a). This recipe can hardly be used in case of GaAs since there is no symmetry operation that converts Ga to As (Figure 1.11b). Therefore, GaAs is non-centro-symmetric crystal belonging to class $\bar{4}3m$ and revealing significant piezoelectric effect.

Combining local symmetry elements with translations creates novel elements of spatial symmetry – glide planes and screw axes. Therefore, spatial symmetry is a combination of local (point) symmetry and translational symmetry. As a result, 32 point groups + 14 **Bravais** lattices produce 230 space groups describing all possible variants of crystal symmetry, associated with charge distributions, i.e. related to geometrical points and polar vectors. Magnetic symmetry, linked to magnetic moments (axial vectors, see Section 1.2), will be discussed in Chapter 11.

1.2 Symmetry and Physical Properties in Crystals

Crystal symmetry imposes tight restrictions on its physical properties. Term "properties" relates to those that can be probed by regular (macroscopic) optical, mechanical, electrical, and other measurements, averaging over the actual atomic-scale periodicity of physical characteristics. Note that complete spatial symmetry of the crystal is revealed in diffraction measurements using quantum beams (X-rays, neutrons, electrons) with wavelengths comparable with translational periodicity. Note that crystal characteristics, even averaged over many translation periods, show anisotropy which is dictated by the crystal point group. Within this averaged approach, the symmetry constraints are formulated by means of the so-called **Neumann's** principle: the point group of the crystal is a sub-group of the group describing any of its physical properties. In simple words, the symmetry of physical property of the crystal cannot be lower than the symmetry of the crystal: it may be only equivalent or higher.

In practical terms, it means that if physical property is measured along certain direction within the crystal and then the atomic network is transformed according

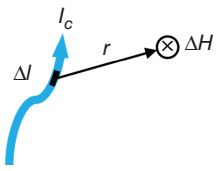

Figure 1.12 Illustration of the **Biot–Savart** law (Eq. (1.7)).

any symmetry element of its point group and measurement repeats, we expect to obtain the measurable effect of the same magnitude and sign as before. Any deviation will contradict particular crystalline symmetry and, thus, the **Neumann's** principle. Using mathematical language, physical properties are, generally, described by tensors of different rank, for which the transformation rules under local symmetry operations are well-known. Tensor rank defines the number of independent tensor indices, *i, k, l, m,…*, each of them being run between 1 and 3, if the 3D space is considered. In most cases, physical property is the response to external field applied to the crystal. Note that external fields are also described by tensors, which are called field tensors to distinguish them from crystal (material) tensors.

Tensors of zero rank are scalars. It means that they do not change at all under coordinate transformations related to symmetry operations. As an example of scalar characteristics, we can mention the mass density of a crystal. Tensor of rank one is a vector. It has one index $i = 1,2,3$, which enumerates vector projections on three mutually perpendicular coordinate axes within **Cartesian** (**Descartes**) coordinate system. It is easy to point out field vectors, for example, an applied electric field, $\mathcal{E}_i$, or electric displacement field, D_i. As crystal vector, existing with no external fields, one can recall the vector of spontaneous polarization, P_i^s, in ferroelectric crystals (see Chapter 12). Spontaneous polarization, as well as polarization, P_i, induced by external electric field, is defined as the sum of elementary dipole moments per unit volume. Note that polarization $\boldsymbol{P}$ is polar vector having three projections, P_i, as e.g. radius-vector $\boldsymbol{r}$ (with projections, x_i). There exist also axial vectors (or pseudo-vectors), i.e. vector products (cross products) of polar vectors, which are used to describe magnetic fields and magnetic moments. In fact, magnetic field, $\boldsymbol{\Delta H}$, produced by the element $\boldsymbol{\Delta l}$ of a conducting wire carrying electric current, I_c, is described by the **Biot–Savart** law:

$$\boldsymbol{\Delta H} = \frac{I_c\,[\boldsymbol{\Delta l} \times \boldsymbol{r}]}{4\pi\, r^3} \tag{1.7}$$

where $\boldsymbol{r}$ is the radius-vector connecting the element $\boldsymbol{\Delta l}$ and the observation point (see Figure 1.12). In turn, magnetic dipole moment, $\mu_{\boldsymbol{d}}$, is defined as an integral over the volume containing the current density distribution $\boldsymbol{J}$:

$$\mu_{\boldsymbol{d}} = \frac{1}{2}\iiint [\boldsymbol{r} \times \boldsymbol{J}]dV \tag{1.8}$$

Axial vectors are considered when analyzing magnetic symmetry and magnetic symmetry groups (Chapter 11).

Tensor of rank 2 has two independent indices $i, k = 1, 2, 3$. As a rule, it linearly connects two vectors, e.g. the vectors of the electric displacement field, D_i, and external electric field, $\mathcal{E}_k$, i.e. $D_i = \sum_{k=1}^{3} \varepsilon_{ik}, \mathcal{E}_k$, as tensor of dielectric permittivity, ε_{ik}, does

(see Chapter 8). Another example is the density of electric current, J_i, and electric field, $\mathcal{E}_k$, connected by the electrical conductivity tensor ρ_{ik}, i.e. $J_i = \sum_{k=1}^{3} \rho_{ik}\mathcal{E}_k$ (see Chapter 4). In further analyses, we will omit the summation symbols and use the reduced record (according to the **Einstein** convention) for tensor relationships, e.g.

$$D_i = \varepsilon_{ik}\mathcal{E}_k \tag{1.9}$$

$$J_i = \rho_{ik}\mathcal{E}_k \tag{1.10}$$

There are two important field tensors of second rank, which are in common use. These are the stress and strain tensors. Stress tensor, σ_{ik}, connects vector of external force, F_i, applied to a certain crystal area, ΔS, and unit vector, $\widehat{n}_k$, normal to this area:

$$F_i = \sigma_{ik}\Delta S\widehat{n}_k \tag{1.11}$$

Based on the mechanical equilibrium of the stressed solid, it is possible to prove that stress tensor (Eq. (1.11)) is symmetric one, i.e. $\sigma_{ik} = \sigma_{ki}$. Regarding strain tensor, it connects the deformation vector, u_i, in the vicinity of a given point and the radius-vector of this point, x_i. Deformation vector determines the difference in the distances between closely located points near x_i in the deformed and non-deformed states of the crystal. To provide local information on the deformed state, strain tensor, e_{ik}, is defined in the differential form:

$$e_{ik} = \frac{1}{2}\left(\frac{du_i}{dx_k} + \frac{du_k}{dx_i}\right) \tag{1.12}$$

Evidently, the strain tensor, defined by Eq. (1.12), is symmetric one, i.e. $e_{ik} = e_{ki}$.

Furthermore, inter-atomic distances within a crystal are also changed upon heating (see Chapter 3). In that sense, a crystal heated up to some temperature, T_1, is in different "deformation" state as compared with its initial state at temperature, T_0. Thus produced relative change in lattice parameters is mathematically equivalent to strain (Eq. (1.12)). Tensor of second rank, which relates e_{ik} to the temperature increase, $\Delta T = T_1 - T_0$ (tensor of rank zero, i.e. scalar), is called as tensor of linear expansion coefficients, α_{ik}:

$$e_{ik} = \alpha_{ik}\Delta T \tag{1.13}$$

Note that both crystal states, at $T = T_0$ and $T = T_{1,}$ are thermodynamically equilibrium states at respective temperatures, and, therefore, no elastic energy is stored in such "deformed crystal," whenever the temperature change is homogeneous across the crystal. The only energy difference between these two states is in free energy, which is temperature dependent.

Tensor of second rank may also connect a scalar and two vectors, as tensor of dielectric permittivity, $\mathcal{E}_{ik}$, does for energy density, W_e, of electromagnetic field within a crystal:

$$W_e = \frac{D_i\mathcal{E}_i}{2} = \frac{1}{2}\varepsilon_{ik}\mathcal{E}_i\mathcal{E}_k \tag{1.14}$$

By using tensor representation for the electric displacement field (see Eq. (1.9)), we find that the energy density is quadratic with respect to the applied electric field, $\mathcal{E}_i$.

Tensor of third rank has three indices $i, k, l = 1, 2, 3$. It connects tensor of second rank and vector, e.g. stress, σ_{ik}, and induced electric polarization, P_i:

$$P_i = d_{ikl}\sigma_{kl} \tag{1.15}$$

as for direct piezoelectric effect, or strain, e_{ik}, and applied electric field, $\mathcal{E}_i$:

$$e_{ik} = d_{lik}\mathcal{E}_l \tag{1.16}$$

for converse piezoelectric effect, both discussed in detail in Chapter 12. Another example is tensor, r_{lik}, of the linear electro-optic effect (the **Pockels** effect, also mentioned in Chapter 12). This tensor of third rank connects the change, Δn_{ik}, of refractive index, n, (which can be described in terms of the second rank tensor) under applied electric field, with the electric field vector, $\mathcal{E}_l$:

$$\Delta\left(\frac{1}{n^2}\right)_{ik} = r_{lik}\mathcal{E}_l \tag{1.17}$$

For the fourth rank tensor, there are several optional ways for its construction. It may connect two tensors of rank 2, e.g. stress, σ_{ik}, and strain, e_{lm}, as the stiffness tensor, C_{iklm} (tensor of elastic modules used in Chapter 3), does:

$$\sigma_{ik} = C_{iklm}e_{lm} \tag{1.18}$$

Similar tensor object, π_{iklm}, is used to describe the photo-elastic effect in crystals, which provides the change of refractive index under applied stress:

$$\Delta\left(\frac{1}{n^2}\right)_{ik} = \pi_{iklm}\sigma_{lm} \tag{1.19}$$

Another possibility is to connect tensor of second rank (e.g. strain tensor, e_{ik}) and two vectors (e.g. quadratic form of electric field, $\mathcal{E}_l\ \mathcal{E}_m$) as for electrostriction effect, g_{iklm}:

$$e_{ik} = g_{iklm}\mathcal{E}_l\mathcal{E}_m \tag{1.20}$$

or changes in refractive index, as a function of quadratic form of electric filed, as for quadratic electro-optic effect, r_{iklm} (see Chapter 12):

$$\Delta\left(\frac{1}{n^2}\right)_{ik} = r_{iklm}\mathcal{E}_l\mathcal{E}_m \tag{1.21}$$

Eqs. (1.20, 1.21) describe the second order (quadratic) effects in the induced strain and change of refractive index, respectively, as a result of electric field application to a crystal. Tensor of rank 4 may also interconnect scalar quantity with two tensors of the second rank, as the stiffness tensor does when one calculates the density of elastic energy, W_{el}, stored within a crystal:

$$W_{el} = \frac{1}{2}\sigma_{ik}e_{ik} = \frac{1}{2}C_{iklm}e_{ik}e_{lm} \tag{1.22}$$

Therefore, using tensor representation of applied stress via induced strain (Eq. (1.18)), we find the density of elastic energy to be quadratic with respect to the induced strain. Tensors of rank higher than 4 describe high-order effects in the interaction between external fields and materials. These effects are regularly weak and, hence, are not discussed here.

Tensors of different ranks are appropriately transformed under local symmetry operations. All these operations can be exemplified as certain rotations of coordinate system, in which tensors are defined. Transformed tensor forms are compared with the initial ones, and, on this basis, symmetry restrictions on physical properties are imposed, to be in accordance with **Neumann**'s principle. Based on this comparison, the zero tensor components can be determined, as well as symmetry-mediated relationships between non-zero tensor components. More information on symmetry aspects in crystals can be found in the dedicated crystallography books.

Additional interesting and important physical phenomenon, also related to symmetry operations, is twinning in crystals. For example, it stands behind the crystallography of ferroelectric domains (see Chapter 12) and is one of the channels of plastic deformation in crystals being competitive with dislocation glide. We stress that in terms of crystallography, twinning always is the result of symmetry operations, but those not belonging to the point group of a specific crystal. More information about twinning in crystals is given in Appendix 1.B.

1.3 Wave Propagation in Periodic Media and Construction of Reciprocal Lattice

With no doubts, leading crystal symmetry is translational symmetry, which is of great importance to the foundations of solid state physics. In particular, it allows us to deeply understand the essential features of wave propagation in periodic media, which influence a majority of physical phenomena in crystals. We start now with the symmetry-based analysis of wave propagation following the ideas of **Leon Brillouin**.

Let us consider, first, the propagation of the plane electron wave, $Y = Y_0 \exp[i(\boldsymbol{kr} - \omega t)]$, in a homogeneous medium. Here, Y_0 is the wave amplitude, $\boldsymbol{k}$ is the wavevector, and ω is the wave angular frequency, whereas $\boldsymbol{r}$ and t are the spatial and temporal coordinates. The phase of plane wave is $\varphi = (\boldsymbol{kr} - \omega t)$, i.e. $Y = Y_0 \exp(i\varphi)$. According to the **Emmy Noether** theorem, the homogeneity of space leads to the momentum conservation law. It means that an electron wave having wavevector, $\boldsymbol{k}_i$, at a certain point in its trajectory, will continue to propagate with the same wavevector since the wavevector, $\boldsymbol{k}$, is linearly related to the momentum, $\boldsymbol{P}$, via the reduced **Planck** constant $\hbar$, i.e. $\boldsymbol{P} = \hbar\boldsymbol{k}$. The latter relationship follows from the de **Broglie** definition of the particle wavelength (**de Broglie** wavelength) via its momentum: $\lambda = \frac{2\pi}{k} = \frac{h}{P}$.

The situation drastically changes for a non-homogeneous medium, in which the momentum conservation law, generally, is not valid because of the breaking of the aforementioned symmetry (homogeneity of space). Consequently, in such a medium, one can find wavevectors, $\boldsymbol{k}_f$, differing from the initial wavevector, $\boldsymbol{k}_i$.

Our focus here is on a non-homogeneous medium with translational symmetry, which comprises scattering centers in specific points, $\boldsymbol{r}_s$, given by Eq. (1.1). Based on the translational symmetry only, we can say that in an infinite medium with no absorption, the magnitude of plane wave, Y, should be the same near each lattice node. It means that the amplitude, Y_0, is the same at all points, $\boldsymbol{r}_s$, whereas the phase,

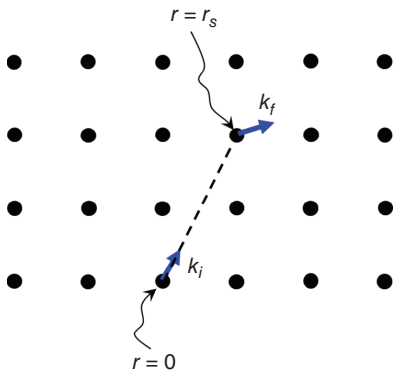

Figure 1.13 Illustration of the wave scattering in a periodic medium.

$\varphi = \boldsymbol{kr} - \omega t$, can differ by an integer number m of 2π.Let us suppose that the plane wave has wavevector, $\boldsymbol{k}_i$, at starting point $\boldsymbol{r}_0 = 0$ and time moment, $t_0 = 0$, and hence $\varphi(0) = 0$. If so, at point $\boldsymbol{r}_s$, the phase, $\varphi(\boldsymbol{r}_s)$, should be equal:

$$\varphi(\boldsymbol{r}_s) = \boldsymbol{k}_f \boldsymbol{r}_s - \omega t = 2\pi m \tag{1.23}$$

Note that the change of the wavevector from $\boldsymbol{k}_i$ to $\boldsymbol{k}_f$ physically means that the wave experiences scattering in point, $\boldsymbol{r}_s$ (Figure 1.13). For elastic scattering (with no energy change):

$$|\boldsymbol{k}_f| = |\boldsymbol{k}_i| = |\boldsymbol{k}| = \frac{2\pi}{\lambda} \tag{1.24}$$

where λ is the electron wavelength. Furthermore, the time interval, t, for wave propagation between points, $\boldsymbol{r}_0 = 0$ and $\boldsymbol{r}_s$, equals

$$t = \frac{\boldsymbol{k}_i \boldsymbol{r}_s}{|\,\boldsymbol{k}_i\,|\,V_p} \tag{1.25}$$

where

$$V_p = \frac{\omega}{|\,\boldsymbol{k}\,|} \tag{1.26}$$

is the phase wave velocity. Substituting Eqs. (1.24–1.26) into Eq. (1.23) yields:

$$\varphi(\boldsymbol{r}_s) = (\boldsymbol{k}_f - \boldsymbol{k}_i)\boldsymbol{r}_s = 2\pi m \tag{1.27}$$

Introducing a new vector, $\boldsymbol{G}$, which is called vector of reciprocal lattice,

$$2\pi \boldsymbol{G} = \boldsymbol{k}_f - \boldsymbol{k}_i \tag{1.28}$$

and combining Eqs. (1.27, 1.28), we find

$$\boldsymbol{G} \cdot \boldsymbol{r}_s = m \tag{1.29}$$

According to Eqs. (1.28, 1.29), different values of $\boldsymbol{k}_f = \boldsymbol{k}_i + 2\pi \boldsymbol{G}$ are permitted in a periodic medium, but only those that provide scalar products of certain vectors, $\boldsymbol{G}$, with all possible vectors, $\boldsymbol{r}_s$, to be integer numbers, m. By substituting Eq. (1.1) into Eq. (1.29), we finally obtain:

$$\boldsymbol{G} \cdot (n_1 \boldsymbol{a}_1 + n_2 \boldsymbol{a}_2 + n_3 \boldsymbol{a}_3) = m \tag{1.30}$$

In order to find the set of allowed vectors, $\boldsymbol{G}$, satisfying Eq. (1.30), the reciprocal space is built, which is based on three non-coplanar vectors $\boldsymbol{b}_1$, $\boldsymbol{b}_2$, and $\boldsymbol{b}_3$. Real (direct) space and reciprocal space are interrelated by the orthogonality (reciprocity) conditions:

$$\boldsymbol{a}_i \boldsymbol{b}_j = \delta_{ij} \tag{1.31}$$

where δ_{ij} is the **Kronecker** symbol, equal to 1 for $i = j$ or 0 for $i \neq j$ ($i, j = 1, 2, 3$). To produce the reciprocal space from real space, we use the following mathematical procedure:

$$\begin{aligned} \boldsymbol{b}_1 &= [\boldsymbol{a}_2 \times \boldsymbol{a}_3]/V_c \\ \boldsymbol{b}_2 &= [\boldsymbol{a}_3 \times \boldsymbol{a}_1]/V_c \\ \boldsymbol{b}_3 &= [\boldsymbol{a}_1 \times \boldsymbol{a}_2]/V_c \end{aligned} \tag{1.32}$$

where V_c stands for the volume of the parallelepiped (unit cell) built in real space on vectors $\boldsymbol{a}_1$, $\boldsymbol{a}_2$, $\boldsymbol{a}_3$:

$$V_c = \boldsymbol{a}_1 \cdot [\boldsymbol{a}_2 \times \boldsymbol{a}_3] \tag{1.33}$$

By using Eqs. (1.32, 1.33), it is easy to directly check that the procedure (1.32) provides proper orthogonality conditions (1.31). For example, $\boldsymbol{a}_1 \cdot \boldsymbol{b}_1 = \boldsymbol{a}_1 \cdot [\boldsymbol{a}_2 \times \boldsymbol{a}_3]/V_c = V_c/V_c = 1$, whereas $\boldsymbol{a}_2 \cdot \boldsymbol{b}_1 = \boldsymbol{a}_2 \cdot [\boldsymbol{a}_2 \times \boldsymbol{a}_3]/V_c = 0$. Certainly, the volume of the unit cell, V_{rec}, in reciprocal space

$$V_{\text{rec}} = \boldsymbol{b}_1 \cdot [\boldsymbol{b}_2 \times \boldsymbol{b}_3] = \frac{1}{V_c} \tag{1.34}$$

is inverse to V_c. To prove this statement, we use the relationship well-known in vector algebra:

$$[\boldsymbol{A} \times \boldsymbol{B}] \times [\boldsymbol{B} \times \boldsymbol{C}] = \{\boldsymbol{A} \cdot [\boldsymbol{C} \times \boldsymbol{D}]\}\boldsymbol{B} - \{\boldsymbol{B} \cdot [\boldsymbol{C} \times \boldsymbol{D}]\}\boldsymbol{A} \tag{1.35}$$

In the reciprocal space, the allowed vectors, $\boldsymbol{G}$, are linear combinations of the basis vectors, $\boldsymbol{b}_1$, $\boldsymbol{b}_2$, $\boldsymbol{b}_3$:

$$\boldsymbol{G} = h\boldsymbol{b}_1 + k\boldsymbol{b}_2 + l\boldsymbol{b}_3 \tag{1.36}$$

with integer projections (hkl), known as **Miller** indices. The ends of vectors, $\boldsymbol{G}$, being constructed from the common origin (000), produce the nodes of a reciprocal lattice. For all vectors, $\boldsymbol{G}$, Eq. (1.30) is automatically valid due to the orthogonality conditions (1.31). We repeat that in the medium with translational symmetry, only those wavevectors, $\boldsymbol{k}_f$, may exist, which are in rigid interrelation with the initial wavevector $\boldsymbol{k}_i$, satisfying Eq. (1.28). Sometimes Eq. (1.28) is called as quasi-momentum (or quasi-wavevector) conservation law in the medium with translational symmetry, which should be used instead of the momentum conservation law in a homogeneous medium. We remind that the latter law means $2\pi\boldsymbol{G} = \boldsymbol{k}_f - \boldsymbol{k}_i = 0$, i.e. $\boldsymbol{k}_f = \boldsymbol{k}_i$.

Note that each vector of reciprocal lattice, $\boldsymbol{G} = h\boldsymbol{b}_1 + k\boldsymbol{b}_2 + l\boldsymbol{b}_3$, is perpendicular to a specific crystallographic plane in real space. This statement directly follows from Eq. (1.29), which defines the geometric plane for the ends of certain vectors, $\boldsymbol{r}_s$, the

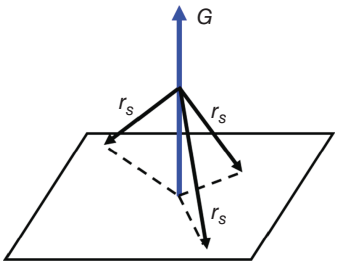

Figure 1.14 Sketch of a crystal plane, normal to the vector of reciprocal lattice, $\boldsymbol{G}$, which contains the ends of vectors, $\boldsymbol{r}_s$, satisfying Eq. (1.29).

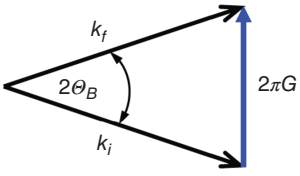

Figure 1.15 Graphical interrelation between wavevectors of the incident ($\boldsymbol{k}_i$) and scattered ($\boldsymbol{k}_f$) waves and the vector of reciprocal lattice, $\boldsymbol{G}$.

plane being perpendicular to the vector $\boldsymbol{G}$ (Figure 1.14). Bearing in mind possible wave diffraction when propagating through a periodic medium, it is worth to introduce a set of parallel planes of this type (i.e. those given by Eq. (1.29)), which are separated by the d-spacing

$$d = \frac{1}{|\,\boldsymbol{G}\,|} = \frac{1}{|\,h\boldsymbol{b_1} + k\boldsymbol{b_2} + l\boldsymbol{b_3}\,|} \tag{1.37}$$

In fact, using graphical representation of Eq. (1.28) (Figure 1.15) and solving the wavevector triangle, we find (with the aid of Eq. (1.24)) that

$$2|\boldsymbol{k}|\sin\Theta_B = \frac{4\pi\sin\Theta_B}{\lambda} = 2\pi|\boldsymbol{G}| \tag{1.38}$$

Substituting Eq. (1.37) into Eq. (1.38), we finally obtain the so-called **Bragg** law:

$$2d\sin\Theta_B = \lambda \tag{1.39}$$

which provides the relationship between the possible directions for the diffracted wave propagation (via **Bragg** angles, Θ_B) and inter-planar spacings (d-spacings), d, in crystals. We stress that if $\lambda > 2d$, **Bragg** diffraction is not possible.

Note that for quasicrystals, the diffraction conditions (like Eq. (1.28)) can be deduced from the quasi-momentum (quasi-wavevector) conservation law in the n-dimensional space (hyperspace, $n > 3$), in which the vectors of reciprocal lattice, $\boldsymbol{G}^{qc}$, are:

$$\boldsymbol{G}^{qc} = \sum_{1}^{n} h_i \boldsymbol{b}^{qc}{}_i \tag{1.40}$$

In case of icosahedral symmetry, $n = 6$, and the set of basis vectors has the following form:

$$\boldsymbol{G}^{qc} = G_0 \sum_{1}^{6} h_i \hat{\boldsymbol{b}}_i^{qc} \tag{1.41}$$

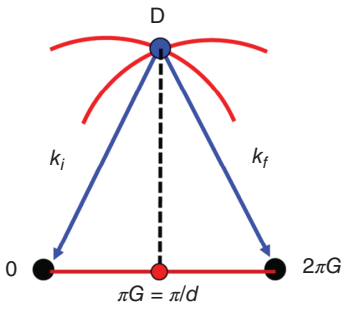

Figure 1.16 The traces of isoenergetic surfaces (red curves) in reciprocal space for the incident ($\boldsymbol{k}_i$) and diffracted ($\boldsymbol{k}_f$) waves. The point of degeneracy of quantum states is marked by the letter **D**.

where G_0 is some constant and $\widehat{\boldsymbol{b}}_i^{qc}$ are unit vectors expressed via the golden ratio (Eq. (1.6)), as:

$$\begin{aligned}
\widehat{\boldsymbol{b}}_1^{qc} &= \frac{1}{1+\tau^2}(1,\tau,0)\\
\widehat{\boldsymbol{b}}_2^{qc} &= \frac{1}{1+\tau^2}(\tau,0,1)\\
\widehat{\boldsymbol{b}}_3^{qc} &= \frac{1}{1+\tau^2}(\tau,0,-1)\\
\widehat{\boldsymbol{b}}_4^{qc} &= \frac{1}{1+\tau^2}(0,1,-\tau)\\
\widehat{\boldsymbol{b}}_5^{qc} &= \frac{1}{1+\tau^2}(-1,\tau,0)\\
\widehat{\boldsymbol{b}}_6^{qc} &= \frac{1}{1+\tau^2}(0,1,\tau)
\end{aligned} \tag{1.42}$$

Using this terminology, regular crystals constitute the largest class, for which $n = 3$ (see Eq. (1.36)).

Considering the latter, we stress that in an infinite periodic medium, the waves having wavevectors $\boldsymbol{k_i}$ and $\boldsymbol{k_f} = \boldsymbol{k_i} + 2\pi\boldsymbol{G}$ are identical from quantum-mechanical point of view that leads to the degeneracy of the corresponding quantum states. The degeneracy point (marked by letter D in Figure 1.16) is located at the intersection of the iso-energetic surfaces (red lines in Figure 1.16) for the incident ($\boldsymbol{k}_i$) and diffracted ($\boldsymbol{k}_f$) waves. Being projected onto vector $\boldsymbol{G}$ in reciprocal space, this point called as the **Brillouin** zone boundary is in the middle between the $\boldsymbol{0}$ and $\boldsymbol{G}$-nodes of the reciprocal lattice (Figure 1.16). Construction based on lines and surfaces normally cutting corresponding vectors of reciprocal lattices in their middles is used to build **Brillouin** zones in two and three dimensions (see Chapter 2). As we also will see in Chapter 2, the degeneracy of states at the **Brillouin** zone boundary is removed by an interaction of electron waves with periodic lattice potential that results in the formation of the forbidden energy zones (gaps). Within these gaps, the electron states do not exist. Therefore, we can say that energy gaps in crystals are formed due to diffraction of free (or almost free) valence electrons, having wavevectors comparable with vectors of reciprocal lattice.

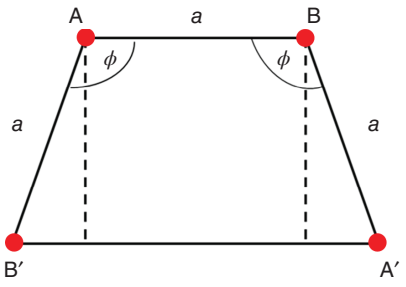

Figure 1.17 Illustration of the restrictions imposed by translational symmetry on permitted types of rotation axes in crystals.

1.A Symmetry Constraints on Rotation Axes

As was already mentioned, translational symmetry imposes tight constraints on possible kinds of rotation axes in crystals. This is one of the strongest and most important results in crystallography. In fact, let us consider the network of equivalent points in space, which are related to each other by translational symmetry (i.e. are produced from some origin by linear combinations of translation vectors, see Eq. (1.1)). Suppose that the rotation axis, which is characterized by the elementary rotation angle ϕ, crosses one of these points (say point A), perpendicularly to the plane of drawing (Figure 1.17). Point B is shifted from point A by translation vector $\boldsymbol{a}$, the distance AB being equal to the translation length, a. Since point B belongs to the same network, the identical rotation axis is passing also through it. Let rotate point B by angle ϕ about the axis passing through point A. In such a way, we receive third equivalent point B′. Repeating this procedure for point A (i.e. rotating it by angle ϕ about the axis passing through point B), we obtain fourth equivalent point A′. Being equivalent, all four points belong to the same network. It means that the distance A′B′ should be an integer number of translations, a (since vector $\mathbf{A'B'}$ is parallel to vector $\mathbf{AB} = \boldsymbol{a}$), i.e. $A'B' = pa$, where p is an integer. On the other hand, by considering the geometry in Figure 1.17, one finds that $A'B' = AB + 2AB' \cdot \sin(\phi - 90°)$. Using $AB = AB' = a$ yields $pa = a + 2a \cdot \sin(\phi - 90°)$, and finally:

$$\cos\phi = \frac{1-p}{2} \tag{1.A.1}$$

Restrictions imposed on possible types of rotation axes by Eq. (1.A.1), mathematically follow from two conditions: $|\cos\phi| \leq 1$ and integer numbers of p. Possible values of $\cos\phi$ and p, as well as the order of the axis, $n = 360°/\phi$, are given in Table 1.2.

First numerical line in Table 1.2 contains trivial symmetry element, i.e. rotation axis *1* ($n = 1$, $\phi = 360°$). It is trivial since each geometrical figure transforms into itself under rotation by 360°. According to Table 1.2, as non-trivial elements, there are only four different rotation axes in crystals, which are compatible with translational symmetry: *2* ($n = 2$, $\phi = 180°$), *3* ($n = 3$, $\phi = 120°$), *4* ($n = 4$, $\phi = 90°$), and *6* ($n = 6$, $\phi = 60°$).

As next important question, we ask: how many rotation axes of the same high order (*3*, *4*, or *6*) can simultaneously exist in a crystal? To address it, let take one

Table 1.2 Possible types of rotation axes permitted by translational symmetry.

p	$\cos\phi$	ϕ	$n = \frac{360^\circ}{\phi}$
−1	1	360°	1
0	½	60°	6
1	0	90°	4
2	−½	120°	3
3	−1	180°	2

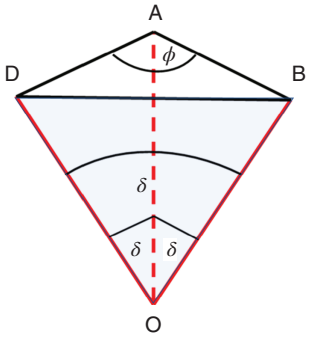

Figure 1.18 Illustration of the simultaneous appearance of several high-order rotation axes in a crystal.

n-fold axis, marked as OA in Figure 1.18, and add to it another axis of this kind (OB) inclined by angle δ. Then, we can rotate the axis OB around OA by the elementary rotation angle, $\phi = 360^\circ/n$, and produce the third axis, OD. The duplication procedure can be continued. However, all these axes are equivalent and, thus, the angles between them should be equal δ. The latter condition imposes strong restrictions on possible configurations of equivalent rotation axes in crystals and angles between them.

In fact, it follows from triangle DOB that DB = 2·DO·sin(δ/2). The plane of triangle DAB is perpendicular to the axis OA and hence the angle ∠ OAD = 90°. If so, DA = DO·sinδ and from triangle DAB, the segment DB = 2·DA·sin(ϕ/2) = 2·DO·sin(ϕ/2)·sin δ . Comparing two expressions for segment DB, given in this paragraph, yields $\sin\frac{\delta}{2} = \sin\frac{\phi}{2}\sin\delta$, or

$$\cos\frac{\delta}{2} = \frac{1}{2}\left[\sin\left(\frac{\phi}{2}\right)\right]^{-1} \tag{1.A.2}$$

For a threefold rotation axis (axis *3*, $\phi = 120^\circ$), Eq. (1.A.2) predicts that $\cos\frac{\delta}{2} = \frac{1}{\sqrt{3}}$ and, correspondingly, cos$\delta = -1/3$. This angle, $\delta = 109.47^\circ$, is between the space cube diagonals, e.g. between the [111]- and [$\overline{1}$11]-diagonals. In other words, crystal symmetry permits the existence of single axis *3*, as follows from translational symmetry, or the simultaneous existence of four such axes (no more, not less), arranged in 3D space as spatial diagonals of a cube. The arrangement of four threefold rotation

axes is the leading combination in the cubic symmetry system, existing in all five its classes (point groups) (Table 1.1).

For a fourfold rotation axis (*4*, $\phi = 90°$), Eq. (1.A.2) gives $\cos\frac{\delta}{2} = \frac{1}{\sqrt{2}}$, i.e. $\delta = 90°$. This is the angle between cube edges. In other words, crystal symmetry permits the existence of single axis *4*, or three such axes, arranged as cube edges, i.e. with angles $\delta = 90°$ between them. This combination exists in classes 432 and $m\bar{3}m$ of the cubic symmetry system (Table 1.1). In cubic class $\bar{4}3m$, we find three fourfold roto-inversion axes, which combine 90° rotation followed by inversion operation.

For a sixfold rotation axis (*6*, $\phi = 60°$), Eq. (1.A.2) yields $\cos(\delta/2) = 1$, i.e. $\delta = 0$. In other words, crystal symmetry allows the existence of single sixfold axis only in all classes of hexagonal symmetry (Table 1.1).

1.B Twinning in Crystals

As was already mentioned, twinning is very interesting and practically important phenomenon in crystal physics, which is tightly related to specific symmetry operations. The phenomenon of twinning in crystals has been extensively studied due to its emergence in crystal growth and phase transformations and its substantial effect on mechanical, electrical, and optical properties in real crystals. In fact, twinning is one of the key mechanisms of plastic deformation in metals and ceramics. Quite often it serves as a structural basis for different types of ferroelectric domains (see Chapter 12) or structural variants in shape-memory alloys.

In contrast to what we have learned until now, symmetry operations involved into twinning processes are not included into the point group of a particular crystal, in which twinning occurs. Correspondingly, twins are crystal parts (sometimes called individuals), which are transformed into each other under such symmetry operations. In fact, if a specific symmetry element, considered for twinning, belongs to the crystal point group, its application to one crystal part would produce perfect continuation of the crystal, rather than a twin. In principle, every basic symmetry element, introduced earlier in Section 1.1, may serve for twinning, if it does not belong to the point group set for a given crystal. However, most frequently twins are produced by reflection in a mirror plane or by a 180° rotation about the twofold rotation axis perpendicular to the boundary plane between the twinned parts. If a crystal has an inversion center, both operations result in identical twins.

Let us illustrate these considerations by two examples, the first being taken for monoclinic lattice, which is characterized by lattice translations $\boldsymbol{a}$, $\boldsymbol{b}$, and $\boldsymbol{c}$ and angle $\gamma \neq 90°$ between vectors $\boldsymbol{a}$ and $\boldsymbol{b}$. Correspondingly, vector $\boldsymbol{c}$ is perpendicular to both the vectors $\boldsymbol{a}$ and $\boldsymbol{b}$. In monoclinic crystals, containing mirror plane as symmetry element (classes *m* and *2/m*, see Table 1.1), this plane is horizontal, i.e. perpendicular to the $\boldsymbol{c}$-translation (in our setting). Consequently, the planes containing translations $\boldsymbol{a}$ and $\boldsymbol{c}$ or $\boldsymbol{b}$ and $\boldsymbol{c}$ are not mirror planes (Figure 1.19). However, if nevertheless, part of the crystal is produced according to this "forbidden" symmetry operation (as fault during growth or because of stress application), one obtains twins shown in Figure 1.19. The angle between twinned parts equals $180° - 2\gamma$.

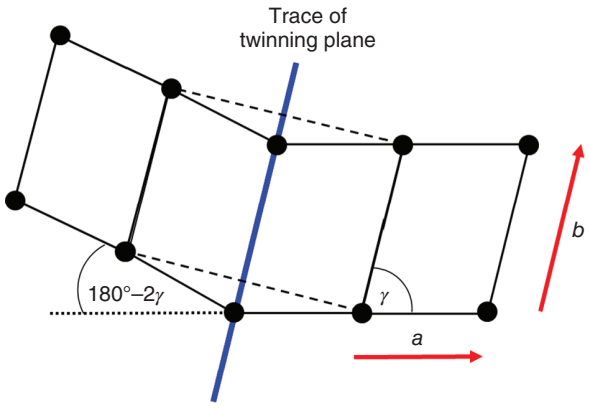

Figure 1.19 Illustration of twin formation in monoclinic lattice via mirror reflection in plane containing the ***b***- and ***c***-translations. The latter is perpendicular to the plane of drawing. The ***a***- and ***b***-translation vectors are indicated by red arrows. Twins are crystal parts located at right-hand and left-hand sides from the trace of the twinning plane (blue solid line).

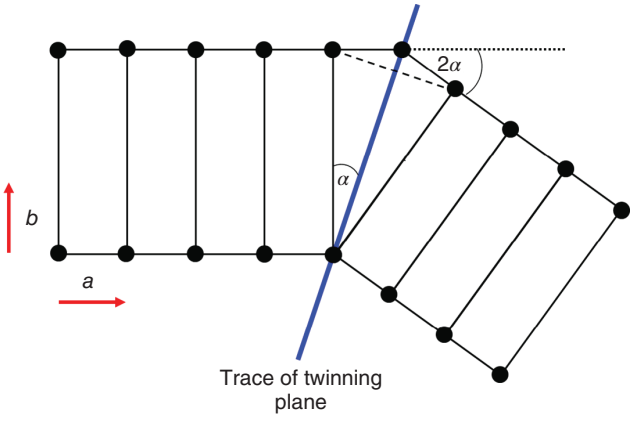

Figure 1.20 Illustration of twin formation in orthorhombic lattice via mirror reflection in plane containing the (***b*** + ***a***)- and ***c***-translations. The latter is perpendicular to the plane of drawing. The ***a***- and ***b***-translation vectors are indicated by red arrows. Twins are crystal parts located at right-hand and left-hand sides from the trace of the twinning plane (blue solid line).

As second example, let us consider orthorhombic lattice with lattice translations ***a***, ***b***, ***c***, being mutually perpendicular to each other. In orthorhombic crystals (classes *222*, *mm2*, and *mmm*, see Table 1.1), the faces of rectangular prism, which represents unit cell, are related to certain symmetry elements. For class *mm2* they are mirror planes, while for class *222* the normals to these planes are the twofold rotation axes. For class *mmm* both assertions are valid. Therefore, if we apply these symmetry operations to one part of the respective crystal, we will obtain its perfect continuation. Situation is changed, if we consider mirror plane, which contains one of the face diagonals of the prism as well as translation vector situated normally to the face chosen. This geometry is shown in Figure 1.20**,** for mirror plane, which contains vectors ***a*** + ***b*** (as face diagonal) and vector ***c***. Application of such mirror plane to a part of the crystal produces twin as is clearly seen in Figure 1.20. If the angle between vector ***b*** and the trace of the twinning plane equals α, then the angle between twinned parts is 2α.

Despite all twins can be considered as being produced by certain symmetry operations, historically twins are also classified with respect to physical processes, through which they appear. In this classification, twins are sub-divided by three categories: growth twins, transformation twins, and deformation twins. Note that these classes not always have lucid boundaries, since crystals may experience deformations also during growth and especially during phase transformations. Note that adjacent ferroelectric domains in perovskite structure (e.g. in $BaTiO_3$ considered in Chapter 12) are good example of transformation twins, if the latter are produced during paraelectric/ferroelectric phase transformation.

Twin boundaries are planar structural defects, which increase free energy of the system, as compared with perfect crystal structure. Correspondingly, twinning planes that require less energy for twin formation are more favorable from energy point of view. For this reason, quite often, twin boundary is a compactly packed atomic plane that prevents re-arrangement of short (and therefore strong) bonds during atomic movements, which accompany the twin formation.